PNAS

Supplementary Information for

A role for endoplasmic reticulum dynamics in the cellular distribution of microtubules

Maria S. Tikhomirova[2], Avihay Kadosh[3], Aksel J. Saukko-Paavola[1], Tom Shemesh[3,*] and Robin W. Klemm[1,2,*]

[1]Department of Physiology Anatomy and Genetics, University of Oxford, Oxford OX1 3PT, UK
[2]Department of Molecular Life Sciences, University of Zurich, 8057 Zurich, CH
[3]Faculty of Biology, Technion-Israel Institute of Technology, Haifa 32000, Israel

*Email: tomsh@technion.ac.il ; Robin.Klemm@dpag.ox.ac.uk

This PDF file includes:

Supplementary text
Figures S1 to S6

Supplementary Information Text

Extended Theory

ER Lattice geometry

In order to investigate the geometry of the tubular ER network, microscopy images were filtered by a random forest-based pixel classifier with intensity and texture features of the CRT signal. The classified images were skeletonized, and junctions were identified based on the number of connected pixels. The skeletonized images were then filtered by a 2D disk filter, resulting in a local density map of 3WJ and tubular processes. The local junction length density, n, is found by ratio of the junction area density to the tubular area density. The local area density of the junctions at each location, ρ, was plotted vs the local length density, n in a log-log plot (see Fig. S4A for data from a representative cell). The data from N=13 cells is well-fitted by a linear regression, corresponding to a relationship $\rho \sim n^a$, with $a = 2.09 \pm 0.05$.

Simulation of the MT-ER system

In this section we describe the details of the simplified system used for our simulations. We treat the sections of the ER as circular sectors, characterized by their sector angle, $\Delta\theta_i$, such that the MTs separating the different sectors correspond to radial lines of length, r. The MT are assumed to be radial, with their locations given by the angles, θ_i, such that $\Delta\theta_i = \theta_{i+1} - \theta_i$. As stated in the main text, the junction length density within each sector, $n_i = N_i / L_i$, is approximately constant. Thus, the local imbalance in the junction length density of neighboring MT-bound ER regions, for each sector, is given by $\Delta n_i \triangleq 2n_i - n_{i+1} - n_{i-1}$. Using the above relations and Eq. (3), we obtain the net 2D pressure for each ER sector, $\sigma^i_{net} = \lambda\left(2n_i - n_{i+1} - n_{i-1}\right)/\left(2\alpha\right)$, equivalent to the net force per unit length acting on the boundary of each sector. The resulting change in the sector angle is given by:

$$\frac{d\left(\Delta\theta_i\right)}{dt} = -\frac{\sigma^i_{net}}{\gamma} = -\frac{\lambda}{2\alpha\gamma}\Delta n_i \qquad \text{(S7)}$$

Where γ is a standard friction coefficient in units of *force*time/length*. Using Eq. (1), we may rewrite Eq. (4) for our circular system if we multiply both sides of Eq. (1) by $r^2/2$. The effective 2D friction coefficient will then be given by $\beta = 2\gamma / r^2$.

When considering the diffusion between neighboring sectors we assume there is a flux of junctions across the sector boundaries, which is proportional to the imbalance in junction area density, $\delta N_i^D = D\left({n_{i+1}}^2 + {n_{i-1}}^2 - 2n_i^2\right)dt$, where the effective 2D diffusion constant, D

, is given in units of $\mu m^2/sec$. The resulting change in n_i is obtained using Eq. (1) and the chain rule:

$$N_i = \frac{A_i n_i^2}{\alpha} \Rightarrow dN_i = \frac{2A_i n_i}{\alpha} dn_i \Rightarrow \delta n_i^D = \frac{dn_i}{dN_i} \delta N_i^D = D \frac{\alpha}{2A_i} \frac{\Delta\left(n_i^2\right)}{n_i} dt \qquad \text{(S8)}$$

The above equation provides us with the equivalent of the diffusion term in Eq. (6).

For our simulations we use 20 circular sectors with the same initial size and junction density. In *Georgiades et al., 2017*, the ER tubules were modelled as hollow cylinders of finite thickness, experiencing a stress of ~60 Pa. Taking the radius and thickness of an ER tubule to be 50 nm and 4nm, respectively, gives $\lambda \simeq 60 fN$. For an MT bundle radius of $r \approx 10\mu m$, $n_0^{\text{exp.}} \approx 0.1\mu m^{-1}$ and $\gamma \approx 25 pN \cdot \text{sec}/\mu m$, the dimensionless coefficients, $\tilde{k}$ and $\tilde{D}$ will be related to their dimensional counterparts as follows:

$$\tilde{k} = \frac{4\alpha\beta A_0}{\lambda n_0} k \triangleq \tau_{sys}^k k \qquad \tilde{D} = \frac{4\beta}{\lambda n_0} D \triangleq \frac{\tau_{sys}^D}{A_{sys}^D} D \qquad \text{(S9)}$$

where $\tau_{sys}^k \simeq 3000\ sec$ and $\tau_{sys}^D / A_{sys}^D \simeq 335\ sec \cdot \mu m^{-2}$. For each sector, the diffusion of junctions occurs through its interface with the neighboring sectors, such that $A_{sys}^D \simeq 2r \cdot d_{MT}$, where d_{MT} is the diameter of the MT bundle separating between the sectors. Using $d_{MT} \approx 0.5\mu m$, we get $\tau_{sys}^D \simeq 3350\ sec$, which is comparable to $\tau_{sys}^k \simeq 3000\ sec$.

Our simulations are implemented in Matlab. The initial state consists of 20 sectors of the same area and junction length density. The dynamics of the system is then obtained using Eqs. (6)-(7) and Eqs. (S1)-(S2). The time unit in our simulation corresponds to ~30 seconds. For a proper realization of the system dynamics, we take small time steps of 0.3 seconds. In addition, we introduce a short range repulsive interaction which becomes dominant below widths that are comparable to the thickness of the MT boundaries, in order to avoid the total collapse of a sector and MT boundaries intersection. In this way, we assure the convergence of the simulation to a steady state within a reasonable time, comparable to the characteristic times of Eq. (S3). We perform the simulation for a range of k, D and n_0. For each choice, we obtain the mean steady state value of the bundling parameter, $\zeta \triangleq \text{std}(\{\Delta\theta_i\}_N) \Big/ \left(\text{mean}(\{\Delta\theta_i\}_N)\sqrt{N}\right)$.

Next, we estimate the maximal force acting on a MT boundary between negihboring sectors. We estimate the maximal junction length density by considering ER tubules which are only twice as long as their diameter (L_{tube}~200nm), giving $\Delta n_{\max} \approx 5/\mu m$. Using $r \approx 10 - 20nm$ and $\lambda \approx 60 fN$, we obtain using Eq. (S1): $F_{\max}^{MT} \approx \left(\lambda r \Delta n_{\max}\right) / \left(2\alpha\right) \approx 10 - 20 pN$.

Finally, we wish to assess the temporal variability in the average junction length density and see whether our simulation results are in qualitative agreement with the results in Fig. (5F). To this end, we perform a scan over a wide range of k and η values and obtain the temporal coefficient of variability, $C_v(n_i) \triangleq std\left(\{n_i\}_t\right) / mean\left(\{n_i\}_t\right)$, for the junction length density in each sector. The time averaging is performed over a wide sample of 60 seconds

intervals, after the system reached its steady state, in accordance with the measurement times reported in Fig. 5. The results are reported in Fig. S4B. The dimensionless noise amplitude is defined as, $\tilde{\eta} \triangleq \sqrt{\tau_{sys}^{k}} \cdot \eta$ and $\tilde{k}$ is the same as in Eq. (S3). We realize that a reduction in the equilibration rate, $\tilde{k}$, leads to both enhanced MT bundling and increased temporal variability, as observed experimentally (Fig. S4B).

Supplemental Material and Methods

Cell culture

COS7 are green monkey kidney cells, and were a kind gift from Tom Rapoport, HHMI, Harvard Medical School. ATL2,3 dKO cells were a gift from Junjie Hu (Chinese Academy of Sciences, Beijing, China) and Yusong Guo (The Hong Kong University of Science and Technology, Hong Kong, China).

All cells were cultured at 37˚C and 5% CO_2 in Dulbecco's Modified Eagle Medium (DMEM, Thermo Fisher Scientific, cat. Nr. 41965-039) containing 25 mM glucose, and glutamine, with 10% Fetal Bovine Serum (FBS, Sigma-Aldrich, cat. N F7524).

RNAi knock-down experiments

The following siRNAs were dissolved in nuclease free ddH_2O to 20 µM and stored at -20˚C (Silencer Select, Thermo Fisher Scientific, cat. Nr. 4392420, ATL3: s24756, ATL2: s34586, LNP: s37454). For reverse transfections experiments the siRNAs were diluted 1:30 to 0.03 µM in OptiMEM (Life Technologies, cat. Nr. 11058-021) and mixed 1:1 with RNAiMAX (Thermo Fisher Scientific, cat. N. 13778075) which was pre-diluted 1:125 in OptiMEM. COS7 cells were trypsinized and diluted in DMEM to 950 cells/ 80µl. 40 µl of the siRNA mixture was added to each well of 96-well plate and 80 µl of cells in DMEM were seeded on top, so that the final concentration of siRNA was 5 nM. In total 950 cells were seeded per well. The cells were allowed to settle to the bottom of the imaging plate at room temperature and then cultured for 72 hours as described above. All volumes were tripled for experiments in 12-well plates.

Antibodies

The following primary antibodies to the specified proteins were used: ATL2 (Proteintech cat. N. 16688-1-AP), ATL3 (Proteintech, cat. Nr. 16921-1-AP), calreticulin (Abcam, cat. Nr. ab2907), pericentrin (Abcam, cat. Nr. ab4448), y-tubulin (Sigma-Aldrich, cat. Nr. T6557-0.2ML), LNP (Sigma- Aldrich, cat. Nr. HPA014205-100UL), vimentin (Abcam, cat. Nr. ab92547), α-tubulin (Sigma- Aldrich, cat. Nr. MAB3408), K40-acetyl γ-tubulin (Abcam, cat. Nr. ab24610).

The following secondary antibodies were used at 1:500 dilution in PBS 1% BSA: anti-mouse Alexa Fluor 488 (Life Technologies, cat. N. A21202), anti-mouse Alexa Fluor 568 (Life Technologies, cat. N. A10037), anti-rabbit Alexa Fluor 488 (Life Technologies, cat. N. A21206) and anti-rabbit Alexa Fluor 568 (Life Technologies, cat. N. A10042). Actin was stained with Alexa Fluor 568 phalloidin (Fisher Scientific, cat. N. A12380).

DNA plasmids

pGFP-EB1 was a gift from Lynn Cassimerus (Addgene plasmid #17234)(1).
GFP-ATL1 was produced by PCR amplification of ATL1 from phage2-mcherry-ATL1, which was a gift from Tom Rapoport (Addgene plasmid #86678) (2), using the following oligonucleotides 5'-TAAGCACTCGAGGCATGGCCAAGAACCGCAGGG-3' (F-GFPATL1) and 5'-TGCTTAGGTACCTTACATTTTTTTCTTTTCTGATTG-3' (R-GFPATL1) as forward and reverse primers, respectively. The PCR product was digested with the restriction enzymes *Xho*I and *Kpn*I and ligated into mEGFP-C1 which was linearized with the same enzymes. mEGFP-C1 was a gift from Michael Davidson (Addgene plasmid #54759).
ss-CRT-mCherry-KDEL (mCherry-ER3) was a gift from Michael Davidson (Addgene plasmid #55041).
mycATL1K80A was a kind gift from Craig Blackstone (Massachusetts General Hospital and Harvard Medical School, Boston, MA, USA, (3)).

Tracking of EB1 on MT +TIPs

The cells were transfected with pEGFP-EB1 (addgene #17234) and subjected to live cell imaging as described above. EB1 +TIPs were extracted using the plusTipTracker, and the dynamics were quantified as described by Applegate et al. (4).

Immunofluorescence

Cells were fixed for 15 min at 37˚C using pre-warmed 4% paraformaldehyde (Electron Microscopy Sciences, cat. N. 15711) in phosphate buffer saline (PBS), and were then washed three times with PBS. Permeabilization was done for 8 min with 0.1% Triton X-100 (Thermo Scientific, cat. N. 28314) in PBS, and washed three times with PBS. Subsequently, the cells were blocked with 2% bovine serum albumin (BSA, Sigma-Aldrich, cat. N. A3912-100G) in PBS for 30 min, then washed with PBS three times. Primary and secondary antibodies were diluted in PBS containing 0.1% CS as specified below. Incubation with the respective antibodies was done for 45 min followed by washing with PBS three times. After that the nuclei were stained with 4',6-Diamidine-2'-phenylindole dihydrochloride (DAPI, Invitrogen, cat. N. D1306) at concentration of 0.4 µl/ml for 10 min and subsequently washed three times with PBS. Finally, to determine the cell outline, the total protein in the cells was stained using Alexa Fluor-647 N-hydroxysuccinimide (NHS) ester (also described as succinimidylester-647 (SE-647), Thermo Scientific, cat. N. A37573) in carbonate buffer to a final concentration of 0.5 ng/ml, incubated for 5 min and washed with PBS three times.

Microscopy

Fixed cells were imaged with a spinning disk microscope (Yokogawa, Cell Voyager 7000) equipped with an enhanced CSU-W1 spinning disk (micro-lens enhanced dual Nipkow disk confocal scanner, wide view type), a 40x Olympus objective with 0.95 NA, and Neo sCMOS cameras (Andor, 2,560 Å, and ca. 2,160 pixels). 10 z-planes were acquired per site, which were maximum intensity projected (MIP) unless stated otherwise. Images were collected at 4 different wavelengths (405nm, 488nm, 567nm, 647nm). In figure 1, the same settings were used except that the images were acquired with a 60x, 1.2 NA Olympus water immersion objective.

Live-cell imaging was performed using a VisiScope spinning disk confocal system (Nikon Eclipse Ti Spinning Disk, VisiScope Confocal Cell explorer), equipped with a 63x oil immersion objective with NA 0.94 and a sCMOS PCO Edge 5.5 camera. Cells were placed into a Labtek-chamber at 37˚C and supplied by 5% CO2 during the entire imaging time. Cells were tracked either using recombinantly expressed fluorescently tagged markers, or Hoechst (800nM) added 15 min prior to imaging. Acquisition time is specified in the main text.
Stimulated emission depletion (STED) microscopy was done on the CLSM – Leica SP8 inverse STED3x setup using a 93x glycerin, NA 1.3 objective with motor correction.
Microscopy of the ATL2,3 knock out cells:
Images for parts of Fig. 6 and S6 were captured on an Olympus SpinSR10 spinning disc confocal system fitted with an Olympus IX-83 frame, a Yokogawa CSU-W1 SoRa super-resolution spinning disc module, a Photometrics Prime BSI camera and a 60× objective (1.5 NA, UPLAPOHR60x), using Olympus cellSens Dimension software. When indicated images in Figure 6 were then processed using OSR filter (standard) and deconvolved (constrained iterative, maximum likelihood, 5 iterations) using Olympus cellSens Dimension software (version 3.1.1). Figures were prepared using ImageJ (FIJI, Schindelin et al 2012).

Automated image analyses
The image analyses were carried out by executing the CP module-pipelines on a 32-core virtual machine (VM), using GC3Pie as a library in order to submit and control batch jobs to a cloud cluster. For detailed documentation see https://github.com/uzh/gc3pie and https://github.com/gc3pie/gc3pie/blob/master/README.rst.
In general, before the analysis was started, the images were converted from .tif to .png format and the stacks were processed by maximum intensity projection.

A typical CP pipeline was organized as described below:
The modules are provided in https://github.com/pelkmanslab/CellProfilerPelkmans:
LoadImages
IlluminationCorrectionPelkmans for each color channel. To account for technical differences in illumination at different positions of the imaging wells, the images were further illumination corrected.
https://github.com/pelkmanslab/CellProfilerPelkmans/blob/master/Modules/IlluminationCorrectionPelkmans.m

Smooth DAPI and FarRed channels
IdentifyPrimIterative for cell nuclei**.**
DiscardObjectsBySize to clean up the found nuclei**.**
ShrinkObjectsSafely
https://github.com/pelkmanslab/CellProfilerPelkmans/blob/master/Modules/ShrinkObjectsSafely.m
ExpandOrShrink
https://github.com/pelkmanslab/CellProfilerPelkmans/blob/master/Modules/ExpandOrShrink.m

IdentifySecondaryIterative for the cell outline.
https://github.com/pelkmanslab/CellProfilerPelkmans/blob/master/Modules/IdentifySecondaryIterative.m
IdentifyTertiarySubregion for segmentation of tertiary regions such as the cytoplasm**.**
https://github.com/pelkmanslab/CellProfilerPelkmans/blob/master/Modules/IdentifyTertiarySubregion.m
SubtractBackgroundPelkmans for intensity measurements
https://github.com/pelkmanslab/CellProfilerPelkmans/blob/master/Modules/SubtractBackgroundPelkmans.m
MeasureObjectAreaShape for area measurement and shape of nuclei/cell/cytoplasm**.**
https://github.com/pelkmanslab/CellProfilerPelkmans/blob/master/Modules/MeasureObjectAreaShape.m
MeasureObjectIntensity
https://github.com/pelkmanslab/CellProfilerPelkmans/blob/master/Modules/MeasureObjectIntensity.m
MeasureTexture
https://github.com/pelkmanslab/CellProfilerPelkmans/blob/master/Modules/MeasureTexture.m
SaveSegmentedObjects
https://github.com/pelkmanslab/CellProfilerPelkmans/blob/master/Modules/SaveSegmentedObjects.m
CreateBatchFiles to be able to send jobs for further processing in the cloud
https://github.com/pelkmanslab/CellProfilerPelkmans/blob/master/Modules/CreateBatchFiles.m

Additionally, the image analyses pipelines were extended with custom modules when necessary. The following custom modules were used:
FindERCrosses to skeletonize the ER and find 3WJ.
SharpFibers to segment MTs and find their directionality.
IdentifySpots2D to find MT organizing centre (MTOC) and pericentrin (PCNT) spots.
https://github.com/pelkmanslab/CellProfilerPelkmans/blob/master/Modules/IdentifySpots2D.m
Relate was used to associate the identified spots to parent cells.
https://github.com/pelkmanslab/CellProfilerPelkmans/blob/master/Modules/Relate.m
Measurechildren was used to carry out measurements of the related objects.
https://github.com/pelkmanslab/CellProfilerPelkmans/blob/master/Modules/MeasureChildren.m

Segmentation of nuclei and single cells
The nuclei were identified by Otsu's thresholding of the DAPI signal, and the segmented objects were subsequently used as seeding points to identify the cell outline based on the fluorescent succinimidylester (SE-647) signal.
To identify and exclude cells from the datasets that extended over the image borders, or were aneuploidic, or dead cells, we routinely extracted single cell features such as intensity and texture of the DAPI signal as well as shape features of the cells and nuclei,

and used them to train a support vector machine based classifier which is described in the following link https://github.com/pelkmanslab/CellClassificationPelkmans.
The cleaned-up datasets were used for quantitative analyses as described below. Unless specified otherwise, mitotic cells were excluded as well.

Automated ER segmentation
To facilitate the training of the pixel classifier we first improved the local contrast ratios of the images by processing the CRT signal with histogram equalization algorithm provided in Snigbo's ImageMagick: http://im.snibgo.com/customim.htm#equal.
To identify the pixel belonging to the ER we used a random forest based single-pixel classifier which we trained in Ilastik (5). This classifier was then run in headless mode of Ilastik in a batch shell, and applied to all images using a 32-core virtual machine run on a cloud computing platform as described above. This image processing step resulted in an ER map where each pixel in the image was given a probability as belonging to the ER or the background. The probability map was further processed using a CP pipeline yielding a binary ER mask. The probability values ≥ 0.6 were set to 1 (=ER), and <0.6 to 0 (=background). The mask was segmented in all cells that were segmented as defined in previous CP steps. The ER mask belonging to a single cell was then skeletonized, cleaned from artifacts using different morphological operations (built-in and custom designed filters for erosion/dilation).
In brief, the following opening filter was applied (bwareaopen(img,20)) then a morph filter with skeletonize option (bwmorph(imgClean,'skel', Inf)), and then the skeleton was thinned to one pixel by applying (bwmorph(skelimg,'thin')). After that the 3WJs were identified as branch points (bwmorph(skel, 'branchpoints')). To clean the points an additional set of morphological filters with different kernel shape was applied as follows:

```
skel=imclose(skel,1);
skel=bwmorph(skel,'thin');
skel=imclose(skel,[1 1;1 1]);
skel=bwmorph(skel,'thin');
skel=imclose(skel,[1 1 1;1 1 1]);
skel=bwmorph(skel,'thin');
skel=imclose(skel,[1 1 1 1;1 1 1 1]);
skel=bwmorph(skel,'thin');
skel=bwareaopen(skel,5);
```

Open tubule end points were identified using bwmorph(skel, 'endpoints') and the distance between the 3WJs was determined by "bwdistgeodesic(skel,find(cross),'quasi')".

Crosspoints (3WJs) and tubule endpoints were identified using in-built MatLab functions bwmorph 'branchpoints' and endpoints'.

The extent of ER tubule bound polygons was identified as the ratio of the outcome values of the matlab function
"regionprops(logical(EmptyArea),'MajorAxisLength','MinorAxisLength')".
To determine the eccentricity of the polygons the value MajorAxisLength was divided by the value MinorAxisLength.

The area of tubules and sheets was calculated simply as sum of pixels of thresholded Ilastik probability maps that were subsequently binarized as described above.

Automated determination of MT orientation by building MT angle maps

After background subtraction, the resolution of the images stained with antibodies to β-tubulin was increased 3-times, i.e. each pixel was divided into a 3x3 matrix. Then the images were convolved with a Laplace of Gaussian (LoG) kernel, in which the Gaussian filter was elongated (eLoG) ([32 32] with sigmas sqrt(3.8) and 10sqrt(3.8)). The images were convolved with 30 different kernels, rotated from 0 to π resulting in 30 response images with an angle difference of 6 degrees between successive images. These data were used to build a MT angle map (MAM) by selecting for each pixel the angle of maximum intensity. The binary images of the MAM were additionally improved by refining the obtained objects using coherence-enhancing diffusion filtering, which expands and connects interrupted MTs. Next, the orientation of each pixel (θ_p) was iteratively compared to its pixel neighborhood (θ_n) defined by a 5x5 matrix. In the final MAM, pixels were only accepted when their orientation (θ_p) was very similar to their neighbors' orientation (θ_n). Similarity was defined as $|\cos(\theta p - \theta n)|>0.97$ were considered a part of a MT "fiber" as in (6)).

Automated cell cycle stage assessment in population of fixed tissue culture cells

To determine the cell cycle stage in fixed population of hundreds of single cells, we first segmented nuclei and single cells using the DAPI and SE-647 signal as described above. To identify cells in S-phase, we additionally labelled replicating DNA with a 15 min pulse of EdU (5-ethynyl-2'-deoxyuridine), which was visualized by click chemistry with an azide labelled fluorophore as per the manufacturer's instructions (Click-iT EdU Alexa Fluor 647 Imaging Kit, Life Technologies, cat. N. C10340).

Measuring the extent of MT co-alignment across entire cells

To assess the extent of MT alignment in cells, we divided random example cells into 100 sectors of equal size as described below and unified them when they contained MTs with similar angle orientation. To subdivide the cells the the weighted center of its nucleus was selected as its cell center; then a small sector of $2\pi/100$ was rotated around the cell center. Two neighboring sectors were combined when the difference of their mean MT angle was smaller than 12 degrees, and if the distribution of all MT-angles within the fused sectors had a standard deviation below 36 degrees.

Automated determination of angles between tubules at 3WJs

To calculate the angles between ER tubules converging at 3-way junctions (3WJs) each crosspoint was cropped into matrix consisting of 10x10 pixels. The crosspoints were only classified as true 3WJ if indeed 3 tubules were emerging. The pixels belonging to tubules converging at the 3WJ were fitted with lines and the angles were calculated between these lines as arctangence of the cross product divided by the dot product of the vectors forming an angle.

Microtubule depolymerisation

To depolymerize microtubules colchicine (Sigma-Aldrich, C3915, dissolved to 10 mM in EtOH and stored in ethanol at -20˚C) was mixed with the cell culture medium to a final concentration of 8 µM. After the indicated incubation time the cells were fixed and processed for immunofluorescence.

Estimating the junction diffusion exponent

To determine the positions of 3WJs, we trained a supervised random forest-based pixel classifier with intensity and texture features of the CRT. The filtered image was skeletonized, and junctions were identified based on the number of connected pixels. In order to determine junction position at sub-pixel resolutions, we fitted a circular mask to the filtered image, using the skeletonized junction position as initial guess. Tracking of individual junctions was performed by a Matlab implementation of the Hungarian optimization algorithm by Jean-Yves Tinevez, (available at https://github.com/tinevez/simpletracker).

Gaps of up to 3 frames were allowed in assigning junctions across time frames, and only tracks spanning 50 time frames or more were selected. The mean square displacement of each track, $\langle r^2 \rangle$, was then calculated and fitted to a power-law : $\left\langle r^2 \right\rangle = D_\alpha t^\alpha$, where α is the diffusion exponent, and D_α is the diffusion coefficient. Tracks of 3WJ in scrambled cells were characterized by a wide distribution of diffusion exponents, with a mean of $\alpha_{SCR} = 0.57 \pm 0.02$ (Fig. S5A, S5C). This value is in good agreement with previous measurements by the Weiss laboratory. Upon ATL depletion, the distribution of diffusion exponents became shifted to lower values, with a mean of $\alpha_{ATL} = 0.42 \pm 0.02$ (Fig. S5B, S5C).

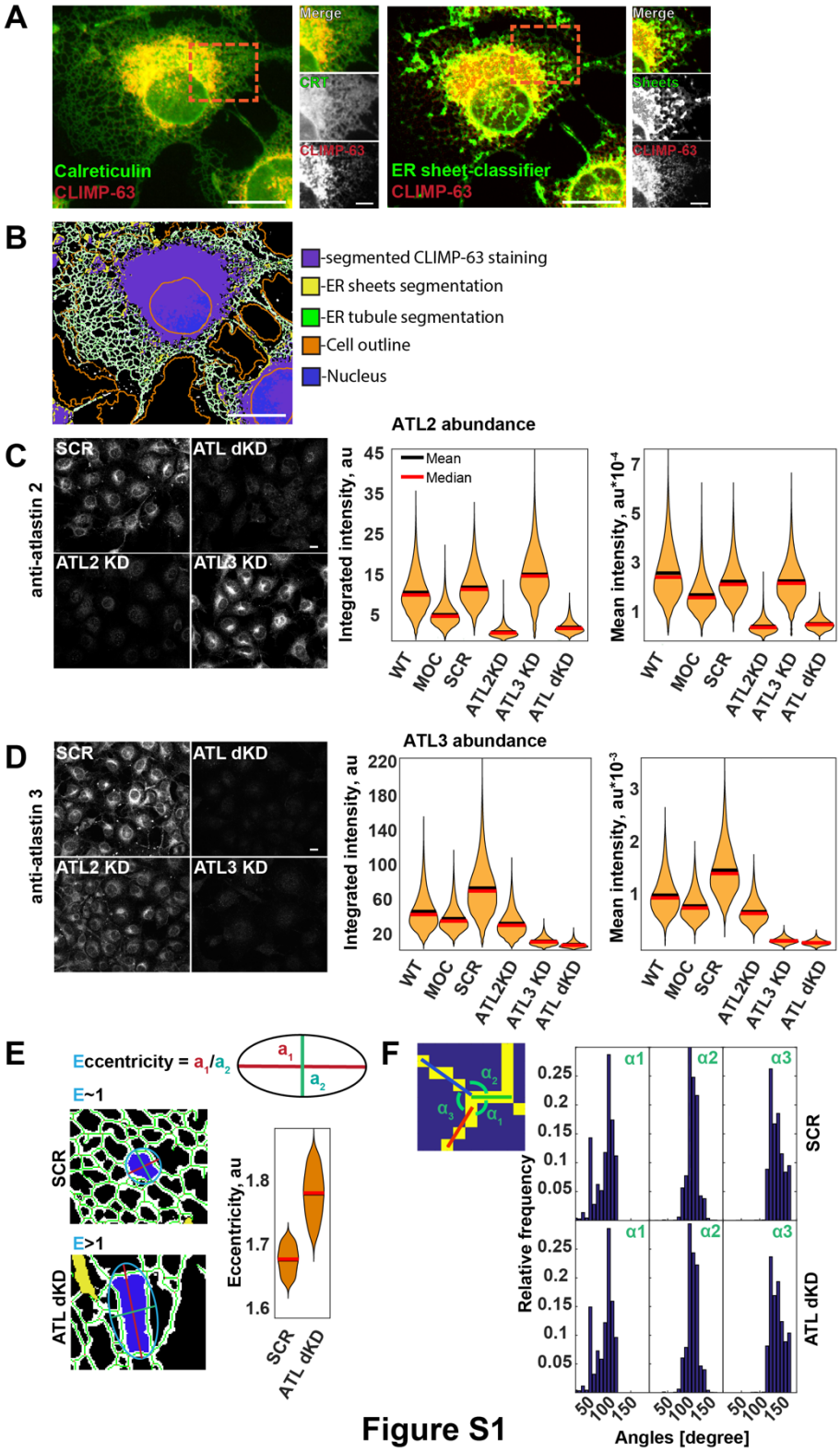
A
Merge
CRT
CLIMP-63
Calreticulin
CLIMP-63
Merge
Sheets
CLIMP-63
ER sheet-classifier
CLIMP-63
B
-segmented CLIMP-63 staining
-ER sheets segmentation
-ER tubule segmentation
-Cell outline
-Nucleus
C
anti-atlastin 2
SCR
ATL dKD
ATL2 KD
ATL3 KD
ATL2 abundance
Integrated intensity, au
Mean
Median
Mean intensity, au*10-4
WT
MOC
SCR
ATL2KD
ATL3 KD
ATL dKD
D
anti-atlastin 3
SCR
ATL dKD
ATL2 KD
ATL3 KD
ATL3 abundance
Integrated intensity, au
Mean intensity, au*10-3
WT
MOC
SCR
ATL2KD
ATL3 KD
ATL dKD
E
Eccentricity = a1/a2
E~1
E>1
SCR
ATL dKD
Eccentricity, au
SCR
ATL dKD
F
α1
α2
α3
Relative frequency
SCR
ATL dKD
Angles [degree]

Figure S1

Fig. S1 Validation of sheet classifier and ATL depletion efficiency; assessment of ER polygon shape, and measurement of angles between tubules at 3WJs.
(A) COS7 cells were analysed by immunofluorescence with antibodies to the luminal ER protein calreticulin and the sheet marker CLIMP-63. The boxed area was enlarged and individual channels are shown at the right. Sheets were automatically segmented and the sheet-pixels identified by the classifier were superimposed with the CLIMP-63 signal. Scale bar, 10 μm (1μm in zooms).
(B) As in (A) but the ER tubules and sheets were segmented. Overlay of ER tubules (white), ER network skeleton (green), CLIMP-63 signal (purple), nucleus (blue), and cell outline (orange).
(C) COS7 cells were treated with scrambled control (SCR), ATL2, ATL3 or ATL2 and 3 specific siRNAs. The cells were subsequently stained with antibodies specific to ATL2 and the cell outline was determined as in Fig. 1B. Single cell ATL2 abundance was determined for all conditions mentioned above including mock transfected cells (MOC). N=5554 (WT), 8841 (MOC), 4789 (SCR), 6359 (ATL2), 1238 (ATL3), 1842(ATLdKD) cells for the conditions indicated in brackets. Scale bar, 10 μm.
(D) As in (C) but the cells were stained with antibodies specific to ATL3 instead. N=5633 (WT), 4665(MOC), 6368 (SCR), 6328(ATL2), 3080(ATL3), 3745(ATLdKD), cells for the conditions indicated in brackets. Scale bar, 10 μm.
(E) Images correspond to boxed area in Fig. 1C. The ER tubule bounded polygons were fitted to an ellipsoid and the eccentricity of the polygons was determined by calculating the ratio of the long (a_1) and the short axes (a_2). Cell number as in Fig. 1D.
(F) The normalized angle distribution of tubules converging at 3WJs was determined. Cell number as in Fig. 1D.

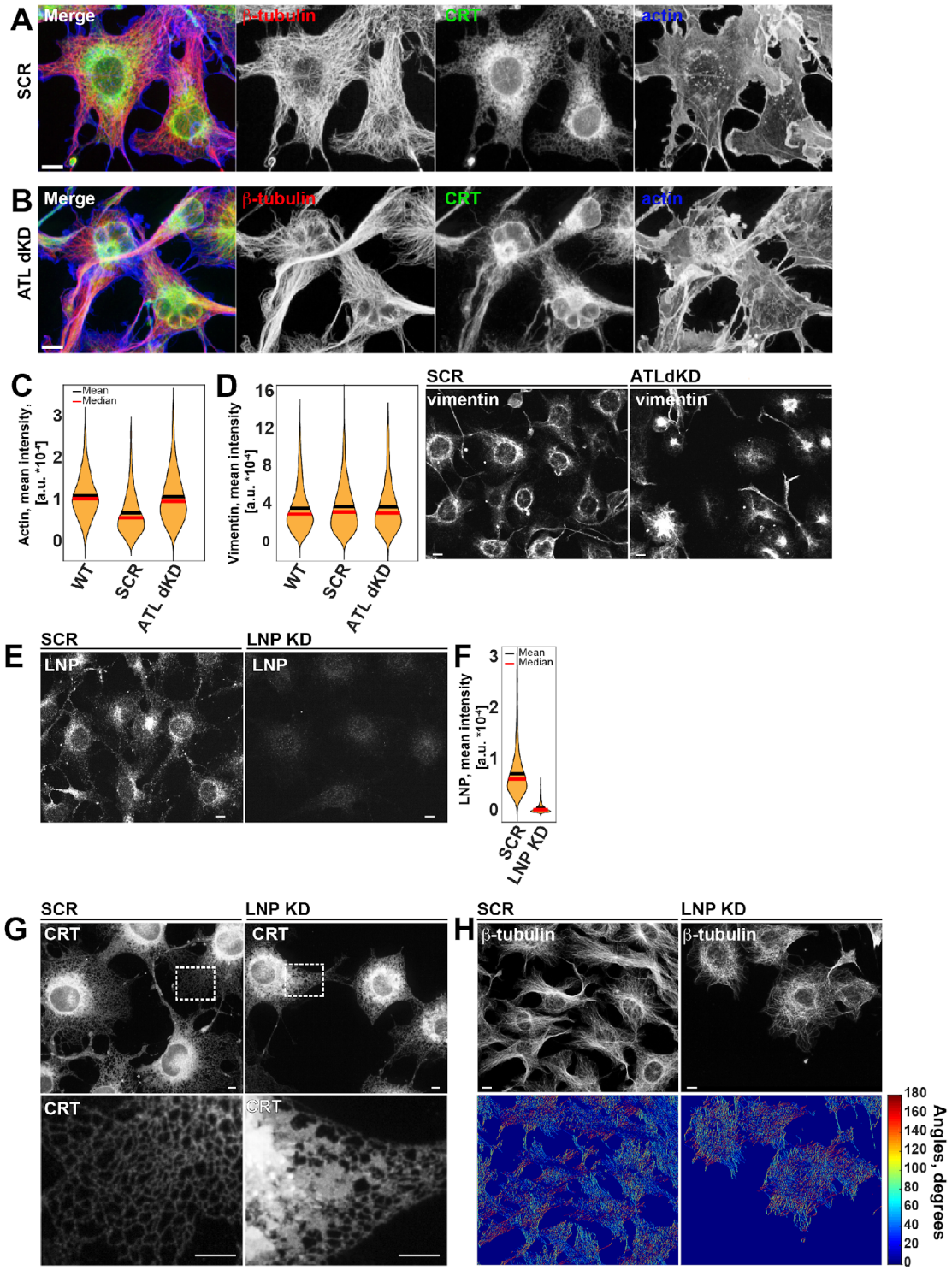
A
Merge
β-tubulin
CRT
actin
SCR
B
Merge
β-tubulin
CRT
actin
ATL dKD
C
Mean
Median
Actin, mean intensity, [a.u. *10⁻⁴]
3
2
1
0
WT
SCR
ATL dKD
D
Vimentin, mean intensity [a.u. *10⁻⁴]
16
12
8
4
0
WT
SCR
ATL dKD
SCR
ATLdKD
vimentin
vimentin
E
SCR
LNP KD
LNP
LNP
F
Mean
Median
LNP, mean intensity [a.u. *10⁻⁴]
3
2
1
0
SCR
LNP KD
G
SCR
LNP KD
CRT
CRT
CRT
CRT
H
SCR
LNP KD
β-tubulin
β-tubulin
180
160
140
120
100
80
60
40
20
0
Angles, degrees

Figure S2

Fig. S2 Actin and Vimentin abundance or distribution do not change in ATLdKD cells and LNP depletion does not lead to MT bundling.
(A) COS7 cells treated with scrambled siRNAs (SCR) were analysed by immunofluorescence with antibodies to β-tubulin, calreticulin and fluorescent phalloidin to visualize F-actin.
Scale bar, 10 μm.
(B) As in (A) but ATL2 and 3 were depleted.
(C) Quantification of mean cellular intensity of actin in untreated wild-type cells (WT), control cells (SCR) or ATL2 and 3 depleted cells (ATL dKD). N=5064 SCR cells, and 1939 ATLdKD cells.
(D) As in (B) and (C) but WT, control cells (SCR) or ATL2 and 3 depleted cells (ATLdKD) were processed for immunofluorescence with antibodies to vimentin. Scale bar, 10 μm
(N= 1549 SCR cells, and 965 ATL dKD cells).
(E) As in Fig. S1D but cells were treated with control (SCR) siRNA oligonucleotides or specific for knock down of LNP (LNP KD). The cells were analysed by immunofluorescence with antibodies to LNP. Scale bar, 10 μm.
(F) Quantification of the mean cellular LNP intensity in SCR and LNP depleted cells (LNP KD)
(N= 4789 SCR cells, and 1066 LNP cells, respectively).
(G) COS7 cells were treated with SCR or LNP specific siRNAs and ER morphology was analysed by immunofluorescence with antibodies to calreticulin (CRT). The boxed areas are enlarged and shown below. Scale bar, 10 μm.
(H) As in **(G)** but β-tubulin was visualized by immunofluorescence. The field of view was processed as described in Fig. 2C. Scale bar, 10 μm.

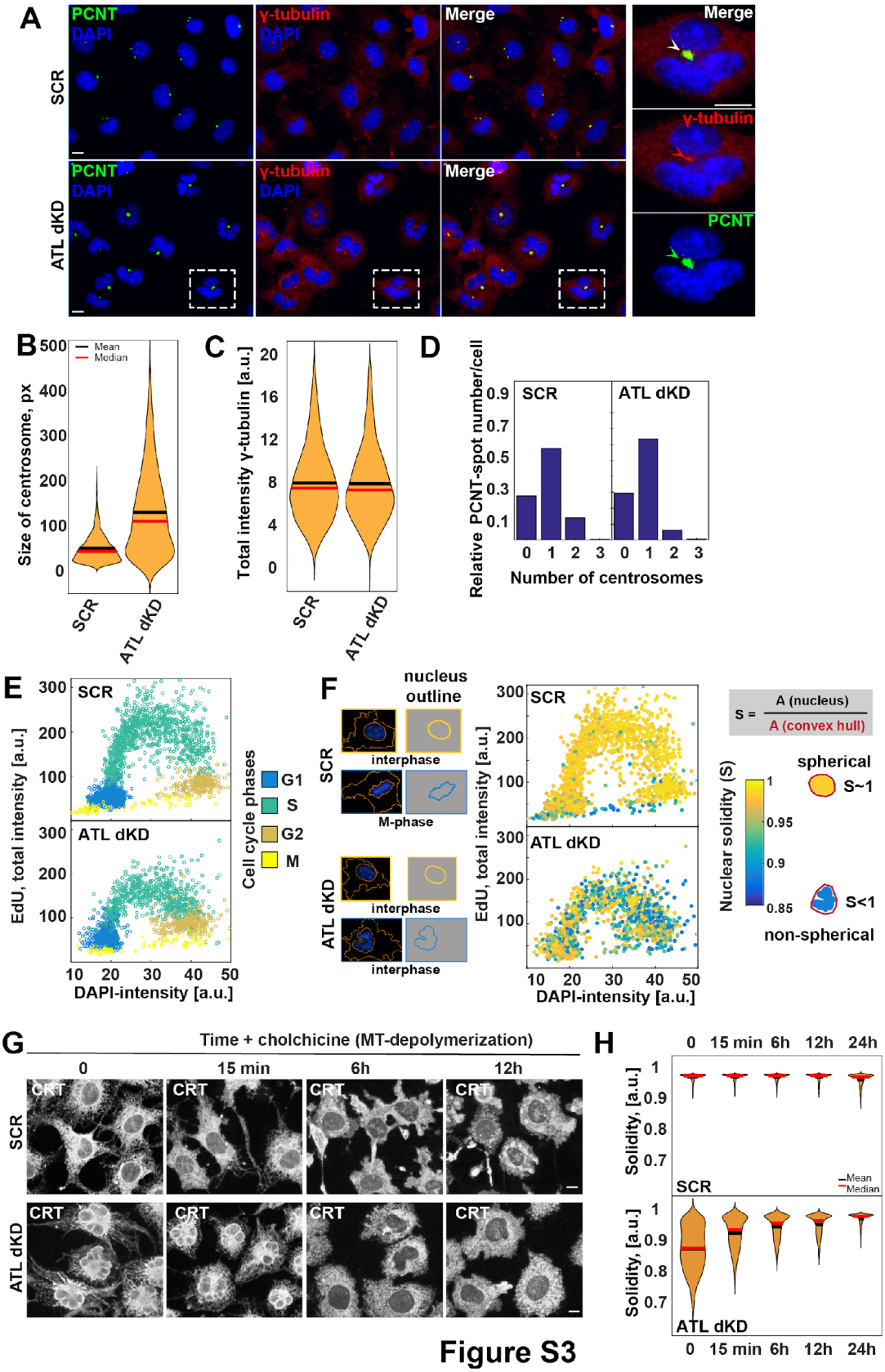
A
PCNT
DAPI
γ-tubulin
DAPI
Merge
SCR
ATL dKD
B
Mean
Median
Size of centrosome, px
C
Total intensity γ-tubulin [a.u.]
D
Relative PCNT-spot number/cell
Number of centrosomes
E
EdU, total intensity [a.u.]
DAPI-intensity [a.u.]
Cell cycle phases
G1
S
G2
M
F
nucleus outline
interphase
M-phase
S = A (nucleus) / A (convex hull)
Nuclear solidity (S)
spherical
S~1
S<1
non-spherical
G
Time + cholchicine (MT-depolymerization)
0
15 min
6h
12h
CRT
H
Solidity, [a.u.]
Mean
Median

Figure S3

Fig. S3 ATL depleted cells have larger centrosomes, progress normally through the cell cycle and nuclear shape changes are rescued after prolonged MT depolymerization.
(A) COS7 cells treated with scrambled siRNAs (SCR) or ATL2 and 3 siRNAs and were analysed by immunofluorescence with antibodies to pericentrin (PCNT) to visualize the centrosome, and γ-tubulin. Scale bar, 10 μm.
(B) As in (A) but the area of the centrosome was compared between SCR and ATL dKD cells.
(C) As in (A) but the total amount of cellular γ-tubulin was quantified.
(D) As in (A) but the centrosomes were segmented based on the PCNT staining and the PCNT spot-count were determined in SCR and ATL dKD cells. (N= 4188 SCR cells, and 3336 ATLdKD cells).
(E) COS7 cells were treated with control siRNAs or with siRNAs to ATL2 and 3 and pulse labelled with ethynyl-deoxyuridine (EdU) to identify cells in S-phase, fixed and then stained with DAPI to quantify the DNA-amount. The cells were processed as described in Material and Methods and classified into G1, S, G2 and M-phase cells. (N= 219207 SCR cells, SCR; and 105873 ATL dKD cells).
(F) as in (E) but the nuclear shape was extracted in addition. The nucleus was segmented based on the DAPI signal and the solidity of the outlined nucleus was determined as a measure of its roundness. The solidity was visualized by colour for each cell that was analysed and plotted on the cell cycle plot made in (E).
(G) COS7 cells were treated with control siRNAs or with siRNAs to ATL2 and 3. Subsequently, MTs were depolymerized for 15 min, 6 hrs and 12 hrs with 8 μM colchicine. The ER was visualized by staining with antibodies to calreticulin (CRT). Scale bar: 10 μm.
(H) as in G but the nuclear solidity was determined at 15 min, 6, 12, and 24 h after colchicine treatment. (N= 6870 SCR, and 5101 ATLdKD cells (t=0h), N= 6308 SCR, and 5058 ATL dKD cells (t=15min), N= 6338 SCR, and 4406 ATLdKD cells (t=6h), N= 4934 SCR, and 3783 ATLdKD cells (t=12h), N= 2615SCR, and 1812 ATLdKD cells (t=24h).

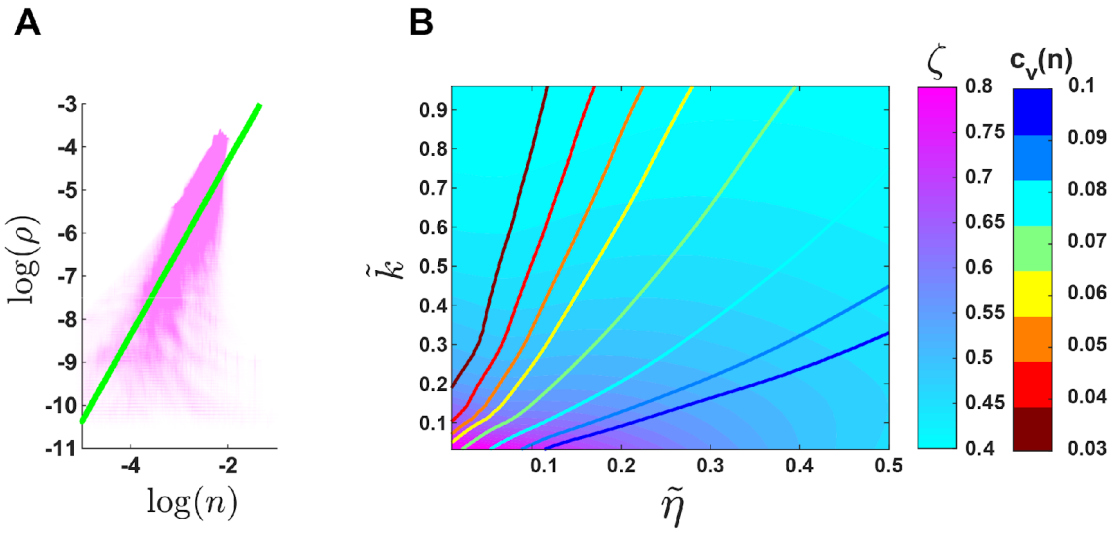
A
B
log(ρ)
log(n)
-3
-4
-5
-6
-7
-8
-9
-10
-11
-4
-2
k̃
η̃
0.9
0.8
0.7
0.6
0.5
0.4
0.3
0.2
0.1
0.1
0.2
0.3
0.4
0.5
ζ
0.8
0.75
0.7
0.65
0.6
0.55
0.5
0.45
0.4
c_v(n)
0.1
0.09
0.08
0.07
0.06
0.05
0.04
0.03

Figure S4

Fig. S4

(A) A log-log scatter plot of representative WT cell. The local area density of 3WJ at each location, ρ, vs the local 3WJ length density, n shown as purple markers. A linear fit is shown in green.

(B) Contour plots of simulated MT bundling parameter, ζ, and simulated temporal variability of junction density, $C_v(n)$, vs. noise parameter, $\tilde{\eta}$, and equilibration parameter, $\tilde{k}$. Each point in the phase space represents the average of 500 simulation instances at steady-state. $\tilde{D} = 0$ for all points.

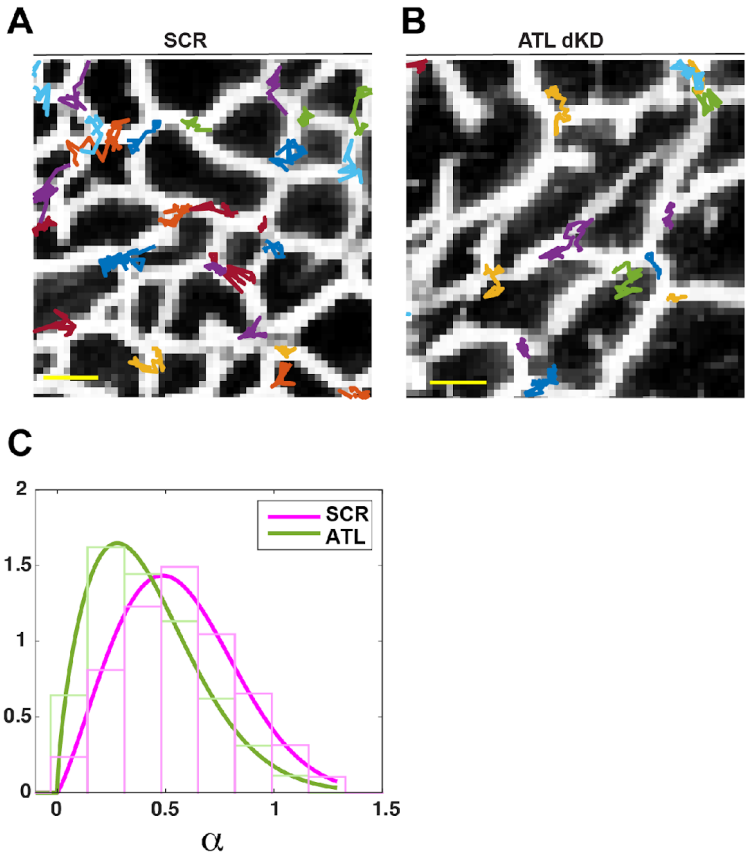

Figure S5

Fig.S5
(A) Individual tracks of 3WJ in a representative ATL dKD cell. Scale bar, 1 μm
(B) Individual tracks of 3WJ in a representative SCR cell.
(C) Distribution of diffusion exponents, α, for ATL dKD cells (green; N=7 cells) and SCR cells (purple; N=8 cells).

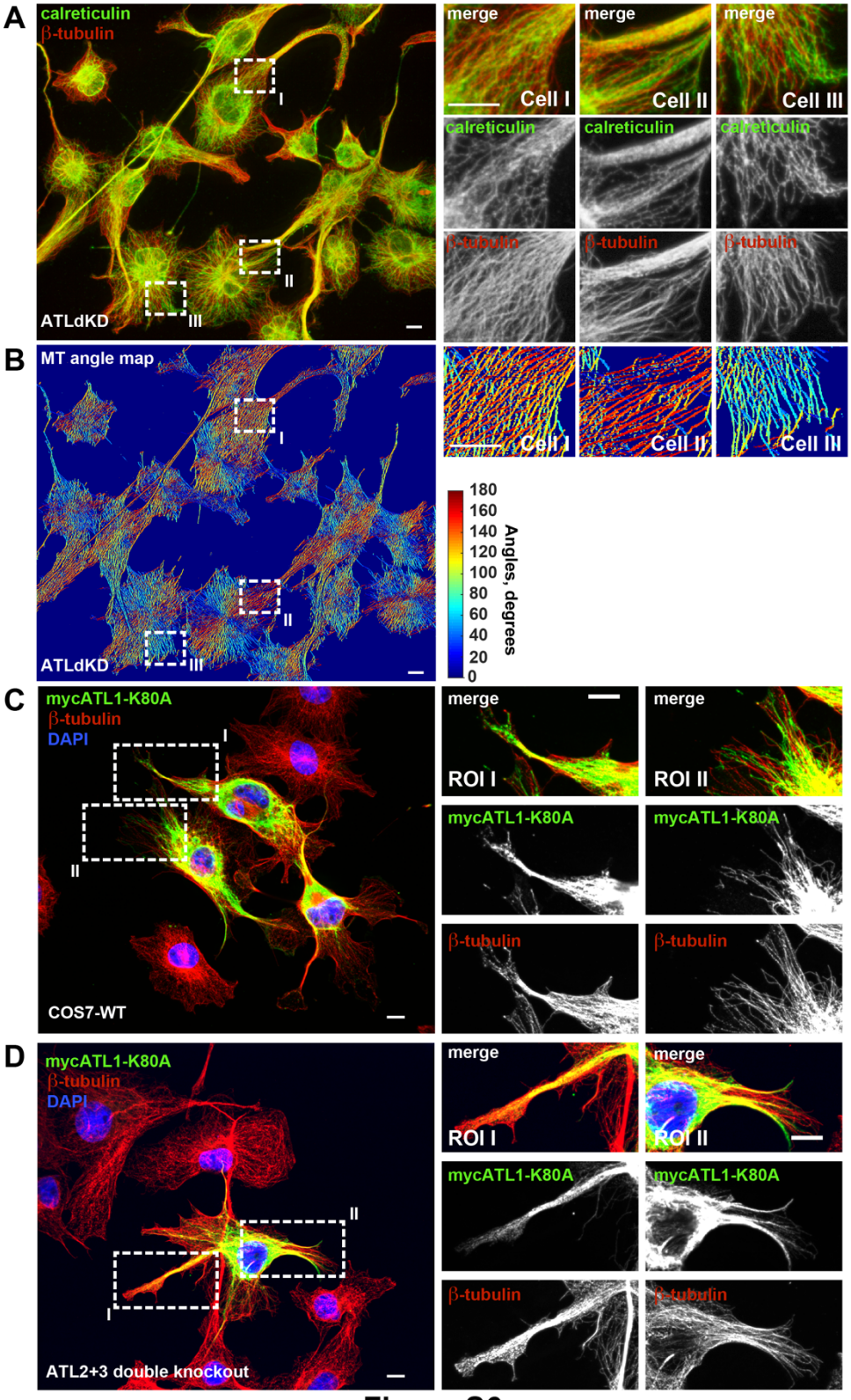
A
calreticulin
β-tubulin
ATLdKD
I
II
III
merge
Cell I
Cell II
Cell III
calreticulin
β-tubulin
B
MT angle map
180
160
140
120
100
80
60
40
20
0
Angles, degrees
C
mycATL1-K80A
β-tubulin
DAPI
COS7-WT
ROI I
ROI II
D
ATL2+3 double knockout

Figure S6

Fig. S6 MTs and the ER co-cluster in bundles upon ATL depletion by RNAi. Expression of dominant negative ATL1K80A leads to the formation of MT bundles and cannot rescue MT distribution in ATL2,3 double knock out cells.
(A) COS7 were treated with siRNAs for ATL2 and 3 (ATLdKD) and analysed by immunofluorescence with antibodies specific to the luminal ER protein calreticulin and β-tubulin. The boxed areas were enlarged and are shown on the right. Scale bar, 10 µm.
(B) As in **(A)** but the MT images were processed as described in Fig. 2C. The MT angles are visualized in colour. Scale bar, 10 µm.
(C) COS7 cells expressing ATL1K80A tagged at its N-terminus with c-myc (mycATL1-K80A) were stained with antibodies specific to c-myc and β-tubulin. Nuclei were visualized with DAPI. Scale bars, 10 µm.
(D) ATL2,3 double knock out cells were stained with antibodies specific to c-myc and β-tubulin. Nuclei were visualized with DAPI. Scale bars, 10 µm.

Supplemental References

1. M. Piehl, L. Cassimeris, Organization and Dynamics of Growing Microtubule Plus Ends during Early Mitosis. *Mol Biol Cell* 14, 916–925 (2003).
2. S. Wang, H. Tukachinsky, F. B. Romano, T. A. Rapoport, Cooperation of the ER-shaping proteins atlastin, lunapark, and reticulons to generate a tubular membrane network. *Elife* 5, 209 (2016).
3. N. Rismanchi, C. Soderblom, J. Stadler, P.-P. Zhu, C. Blackstone, Atlastin GTPases are required for Golgi apparatus and ER morphogenesis. *Hum Mol Genet* 17, 1591 1604 (2008).
4. K. T. Applegate, *et al.*, plusTipTracker: Quantitative image analysis software for the measurement of microtubule dynamics. *J Struct Biol* 176, 168–184 (2011).
5. S. Berg, *et al.*, ilastik: interactive machine learning for (bio)image analysis. *Nat Methods* 16, 1226–1232 (2019).
6. N. Gavara, R. S. Chadwick, Relationship between cell stiffness and stress fiber amount, assessed by simultaneous atomic force microscopy and live-cell fluorescence imaging. *Biomech Model Mechan* 15, 511–523 (2016).